Lithos 380–381 (2021) 105898

Contents lists available at ScienceDirect

Lithos

journal homepage: www.elsevier.com/locate/lithos

Research Article

Reappraisal of the oldest high-pressure type schist in Japan: New zircon U-Pb age of the Kitomyo Schist of the Kurosegawa Belt

Shota Matsunaga [a], Tatsuki Tsujimori [a,b,*], Atsushi Miyashita [c], Shogo Aoki [d,e], Kazumasa Aoki [d], Daniel Pastor-Galán [a,b,f], Keewook Yi [g]

[a] Graduate School of Science, Tohoku University, Sendai 980-8578, Japan
[b] Center for Northeast Asian Studies, Tohoku University, Sendai 980-8576, Japan
[c] Faculty of Science and Technology, Seikei University, Tokyo 180-8633, Japan
[d] Department of Applied Science, Okayama University of Science, Okayama 700-0005, Japan
[e] Graduate School of International Resource Sciences, Akita University, Akita 010-8502, Japan
[f] Frontier Research Institute for Interdisciplinary Sciences, Tohoku University, Sendai 980-0845, Japan
[g] Korea Basic Science Institute, Ochang 28119, Republic of Korea.

ARTICLE INFO

Article history:
Received 16 June 2020
Received in revised form 10 November 2020
Accepted 22 November 2020
Available online 28 November 2020

Keywords:
Late Paleozoic
Subduction metamorphism
'Proto-Japan'
Zircon U–Pb age
Kurosegawa Belt

ABSTRACT

The Kitomyo Schist from Kurosegawa Belt, Shikoku, has been long considered as the oldest records of subduction metamorphism in Japan, based on an early 1970s K–Ar dating of white mica. The schist consists of mafic and pelitic layers and occurs as a tectonic block within serpentinite. Reappraisal of the schist confirmed the schist is characterized by an epidote-amphibolite peak metamorphic facies. The mafic portion is characterized by zoned amphibole + epidote + chlorite + titanite ± phengite ± rutile. The presences of relict rutile surrounded by titanite and the barroisitic cores of zoned amphibole suggest a high-pressure intermediate type metamorphism at the metamorphic peak (P = ~0.8–1.5 GPa and T = ~500–570 °C). The presence of Mn-rich garnet and the lack of biotite, oligoclase and paragonite also support high-pressure intermediate type metamorphism that eliminate the possibility of a typical blueschist-facies metamorphism. New SHRIMP and LA-ICPMS zircon U–Pb geochronology on a pelitic sample show detrital grains of Mesoproterozoic and Early Paleozoic ages, suggesting a maximum deposition age for the trench-fill sediment of ~440 Ma. Also the U–Pb data confirmed ~360 Ma overgrown rims that might have formed during the subduction zone epidote-amphibolite facies metamorphism. Reappraisal revealed that the Kitomyo Schist is not the oldest high-pressure type schist in Japan and rather comparable to the Late Paleozoic Renge Metamorphic Rocks and their equivalents in the Kurosegawa Belt. The Devono–Carboniferous high-pressure metamorphic rocks in Japan might have been paired with their coeval batholiths along the 'Greater South China' margin that was extensively eroded during later tectonic processes.

1. Introduction

The Japanese islands represent the longest record of active 'Pacific-type' orogeny resulting from oceanic subduction, convergence-related arc plutonism, oceanward-accretion, and landward-erosion in the world (e.g., Isozaki, 2019; Isozaki, Aoki, Nakama, & Yanai, 2010; Maruyama, 1997). Japan likely began its 'Pacific-type' oceanic subduction during the latest Neoproterozoic or earliest-most Paleozoic times following the Early Paleozoic high-pressure amphibolites and schists, jadeitites and rodingites found in the Hida-Gaien, Oeyama, Renge and Kurosegawa Belts (e.g., Kunugiza et al., 2017; Maruyama & Ueda, 1975; Tsujimori, 2017; Tsujimori & Liou, 2004; Tsujimori, Liou, Wooden, & Miyamoto, 2005). The gabbroic rocks of hanging wall ophiolite, 'Oeyama Ophiolite' shows 545 ± 3 Ma zircon U–Pb age and 566 ± 95 Ma Sm–Nd whole-rock isochron age (Kimura & Hayasaka, 2019). This very early stage of intra-oceanic subduction zone system has been sometimes described as 'proto-Japan' (e.g., Isozaki, 2019; Isozaki et al., 2010). Isozaki et al. (2010) proposed a schematic oceanic arc–trench cross section of 'proto-Japan' at ~520–480 Ma that delineated '450 Ma (oldest) blueschist', causing misunderstanding about the age of the oldest blueschist-facies (glaucophane-schist facies) metamorphism in Japan. Strictly speaking, Early Paleozoic blueschist-facies metamorphic rocks have not yet been described in Japan (cf., Tsujimori, 2010).

The inferred two oldest localities with high-pressure (H*P*)-type metamorphic rocks in Japan are: (i) the Early Paleozoic kyanite- and paragonite-bearing epidote amphibolite in the Oeyama ultramafic body of the Oeyama Belt (~403–440 Ma Fuko-Pass Metacumulates:

* **Corresponding author at:** Tohoku University, 41 Kawauchi, Aoba-ku, Sendai, Miyagi 980-8578, Japan.
E-mail address: tatsukix@tohoku.ac.jp (T. Tsujimori).

https://doi.org/10.1016/j.lithos.2020.105898
0024-4937/

Tsujimori, Nishina, Ishiwatari, & Itaya, 2000; Tsujimori & Liou, 2004); and (ii) the Early Paleozoic pelitic and mafic schists of the Kitomyo area of the Kurosegawa Belt (~402–445 Ma Kitomyo Schists: Maruyama & Ueda, 1975). Although the Fuko Pass Metacumulates bears a mineralogical indication of H*P* metamorphism most likely having occurred in 'proto-Japan' margin, their protolith, mainly troctolitic igneous cumulates, is not typical of 'Pacific-type' subduction complexes. The Fuko Pass protolith geochemistry as well as the presence of spinel granulite-facies relict minerals suggest an unusually thick oceanic plateau (Tsujimori & Ishiwatari, 2002). In contrast, the Kitomyo Schist has a typical accretionary complex protolith consisting of metabasaltic and metasedimentary rocks. However, no previous descriptions of the schist included a detailed study on index minerals (e.g., glaucophanitic amphibole and/or lawsonite) to determine its metamorphic grade. Moreover, the only geochronological data of the Kitomyo Schist is white mica K–Ar dating from the early 1970s that requires reexamination (e.g., Nishimura, 1998; Tsujimori & Itaya, 1999). We conducted a petrological and geochronological reappraisal of the Kitomyo Schist to understand the first generation of subduction zone metamorphic rocks within the 'proto-Japan' arc–trench system.

2. Geological outline

The Kurosegawa Belt is a composite geotectonic unit, a tectonic mixture of pre-Jurassic components of Southwest Japan (Fig. 1); various fragments of the pre-Jurassic geotectonic units occur as blocks or sheets within a serpentinite-matrix mélange. The Kurosegawa Belt of Shikoku is composed of variable scale serpentinite bodies with Late Paleozoic blueschists (equivalent of the blueschists in the Hida-Gaien, and Renge Belts of the Hida and Chugoku Mountains), Early Paleozoic non-metamorphosed sedimentary rocks, and Early Paleozoic granitoids and rare granulite (e.g., Aoki, Isozaki, Yamamoto, Sakata, & Hirata, 2015; Hada, Ishii, Landis, Aitchison, & Yoshikura, 2001; Maruyama, 1981; Maruyama, Banno, Matsuda, & Nakajima, 1984).

The Kitomyo area is located at the eastern part of the Kurosegawa Belt of Shikoku (Fig. 1). In this area, a fault-bounded serpentinite body (2.5 × 4.5 km) bears amphibolite (or mafic schist) and pelitic schists. The area is about 100 km east of the Ino Formation where pelitic schists associated with glaucophane- and barroisite-bearing schists yields phengite K–Ar ages of 394–352 Ma (four samples) and 327–317 Ma (two samples) (Ueda, Nakajima, Matsuoka, & Maruyama, 1980). According to Maruyama and Ueda (1975), the serpentinite contains brucite and anthophyllite. Both mafic and pelitic schist are characterized by the occurrence of porphyroblastic albite. Maruyama and Ueda (1975) dated white mica (K–Ar) from two psammitic schists (sample 73040305 and 71071401) in Tohoku University, obtaining 445 Ma and 402 Ma, respectively. Based on the age, they considered that the timing of metamorphism was older than 445 Ma.

3. Methods

3.1. Petrography

We selected two samples of the Kitomyo Schist (KTM08 pelitic schist, and KTM11 mafic schist). Textures of polished petrographic thin-sections were observed using a JEOL JSM-7001F field emission-scanning electron microscope (FE-SEM), equipped with an EDS, Oxford INCA X-act energy dispersive X-ray spectrometers at Tohoku University. Major-element quantitative analyses were conducted using a 15 kV acceleration voltage, a 1.4 nA beam current, and a 70 s integration time in the EDS system.

We also analyzed the whole-rock composition of the mafic schist (KTM11) to constrain the nature of its protolith and perform a *P–T* pseudosection model. The analysis was carried out at Activation Laboratories Ltd., Canada, using Code 4Litho Lithogeochemistry Package; the

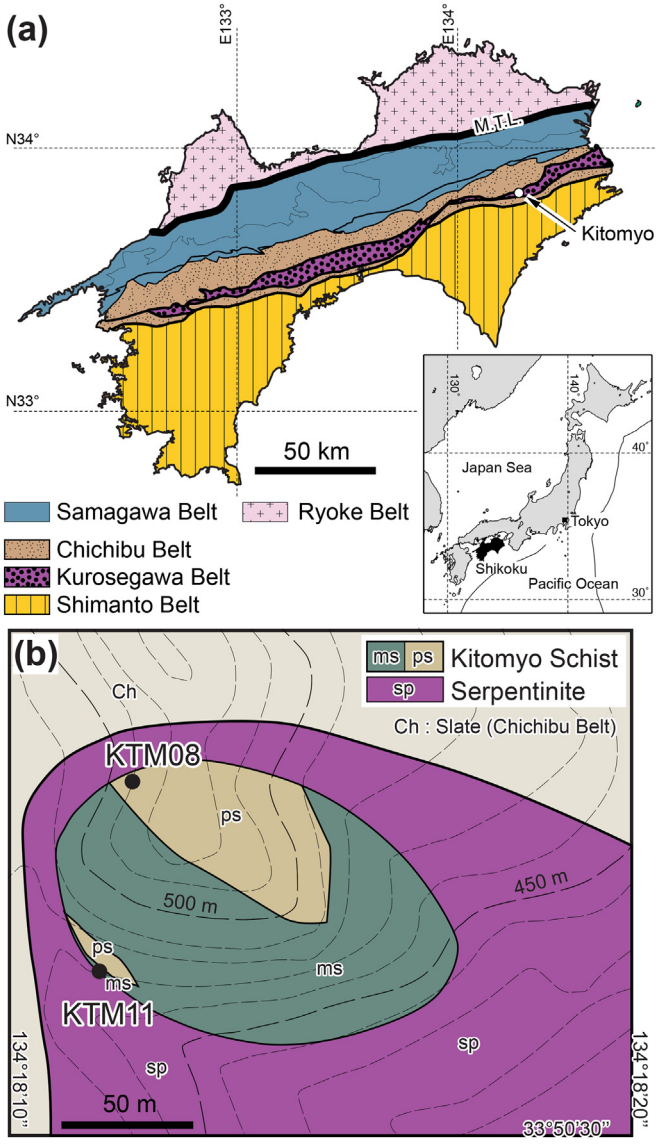

Fig. 1. (a) Simplified geological map of Shikoku delineating the different belts and the location of Kitomyo area, where samples were collected. (b) Detailed geological map of the sampling area (ms: mafic schist. ps: pelitic schist).

package uses lithium metaborate/tetraborate fusion with inductively coupled plasma optical emission spectrometry (FUS-ICPOES) and inductively coupled plasma mass spectroscopy (FUS-ICPMS) for the major- and trace-element analyses, respectively.

3.2. Geochronology

We crushed the samples with a Yasui Kikai Multi Rock Pressure and then sieved them using Nichika Nylon Mesh (#150 [~100 μm] and #100 [~150 μm]) to obtain the proper grain-size for concentrating zircons and phengites. Zircons were concentrated by combining conventional magnetic and heavy liquid methods. Hand-picked zircon grains under a binocular microscope were mounted in 1-in. round epoxy resin (Struers Specifix-40) discs and polished to expose their cores. For the polishing, a Metkon Forcipol 1 V grinder and a 3 M aluminum oxide lapping film were used.

Cathodoluminescence (CL) images of zircon in polished mount of zircon from two sample rocks were observed using a Hitachi S-3400N

SEM, equipped with a Gatan model MiniCL system in Tohoku University. The CL observation was conducted using a 25 kV accelerating voltage and a 90 nA probe current.

In-situ zircon U–Pb dating was carried out in the Okayama University of Science by using a Thermo Fisher Scientific iCAP-RQ single-collector quadrupole ICPMS coupled to a Teledyne Cetac Technologies Analyte G2 ArF excimer laser ablation (LA) system equipped with a HelEx 2 volume sample chamber. The laser ablation of zircons was conducted at the condition of laser spot size of 25 μm with fluence of 1.8 $J \cdot cm^{-2}$ and repetition rate of 5 Hz. Other conditions of LA-ICPMS method are referred to Aoki, Aoki, Tsuchiya, and Kato (2019) and Aoki, Aoki, Tsujimori, Sakata, and Tsuchiya (2020). Zircons were also dated using a SHRIMP IIe/MC instrument at the Korea Basic Science Institute (KBSI) Ochang Center, Korea. Analytical protocols are followed Williams (1998), and reduction of the raw data was undertaken using the software 'SQUID' (Ludwig, 2001). K–Ar age of the phengite separates was determined in the Hiruzen Institute for Geology and Chronology Co. Ltd.; the analytical protocol was followed by Nagao, Nishido, Itaya, and Ogata (1984) and Itaya et al. (1991).

4. Results

4.1. Mineralogical and petrological characteristics

4.1.1. Pelitic schist (KTM08)

Sample KTM08 (Figs. 2a,b) is a quartzo-feldspathic mica schist with quartz-rich layers. Porphyroblastic albite is scattered in the matrix, and it consists mainly of quartz, albite, phengite, secondary chlorite, and minor amount of epidote ($[Fe^{3+}/(Fe^{3+} + Al)] = 0.19–0.24$), tourmaline, ilmenite, and apatite. Oriented lepidoblastic phengite defines a penetrative schistosity. Most garnets (Fig. 2b) ($aalm_{37–68}ggrs_{23–33}ssps_{1–31}Ppyr_{<1}$) are very small (0.03–0.08 mm) subhedral to euhedral grains and included within porphyroblastic albite. Euhedral grains show distinct prograde chemical zoning in spessartine decrease toward the rims. Phengite is lepidoblastic (0.3–1 mm in size) in the matrix and has occasionally intergrown with secondary chlorite; it has a composition with 3.3–3.5 Si atoms per formula unit (a.p.f.u.) for O = 11. Although some phengites in quartz-rich layers are coarse-grained, compositional difference among grain size was not confirmed. Epidote occurs as discrete subhedral grains in association with quartz. The presence of garnet + albite + phengite and the lack of biotite, oligoclase and paragonite suggest that the schist underwent a H*P* intermediate-type metamorphism rather than jadeite–glaucophane type (Miyashiro, 1961). In fact, the mineral assemblage is similar to the garnet zone of the Sambagawa metamorphic belt.

4.1.2. Mafic schist (KTM11)

The sample KTM11(Figs. 2c,d) is a well-deformed, amphibolitic schist that consists mainly of clinoamphiboles and minor amount of epidote ($[Fe^{3+}/(Fe^{3+}+Al)] = 0.28–0.35$), titanite, rutile, phengite and chlorite. Foliation is defined by a preferred orientation of fine-grained acicular pale-greenish actinolite and minor lepidoblastic phengite (3.5–3.6 Si a.p.f.u.). Some coarse-grained blue-greenish barroisitic amphiboles (0.5–1 mm in size; $^{[B]}$Na [Na in the B-site] values reach up to 0.67; Fig. 3) are wrapped around by layers of acicular actinolite (Figs. 2c and 3). Such textural relations indicate that relict, coarser-grained, blue-greenish barroisitic amphibole underwent grain-size reduction by recrystallization during deformation. Some titanites reach up to 1 mm in size and contains abundant rutile (Fig. 2d); such textural relations indicate that relict rutile was replaced by titanite during retrograde metamorphism. The occurrence of relict rutile together with barroisitic amphibole and epidote supports a H*P* intermediate type metamorphism. Moderate to high $^{[B]}$Na content of amphibole is indicative of high-pressure (e.g., Hosotani & Banno, 1986; Nakamura & Enami, 1994; Okamoto & Toriumi, 2005; Otsuki & Banno, 1990).

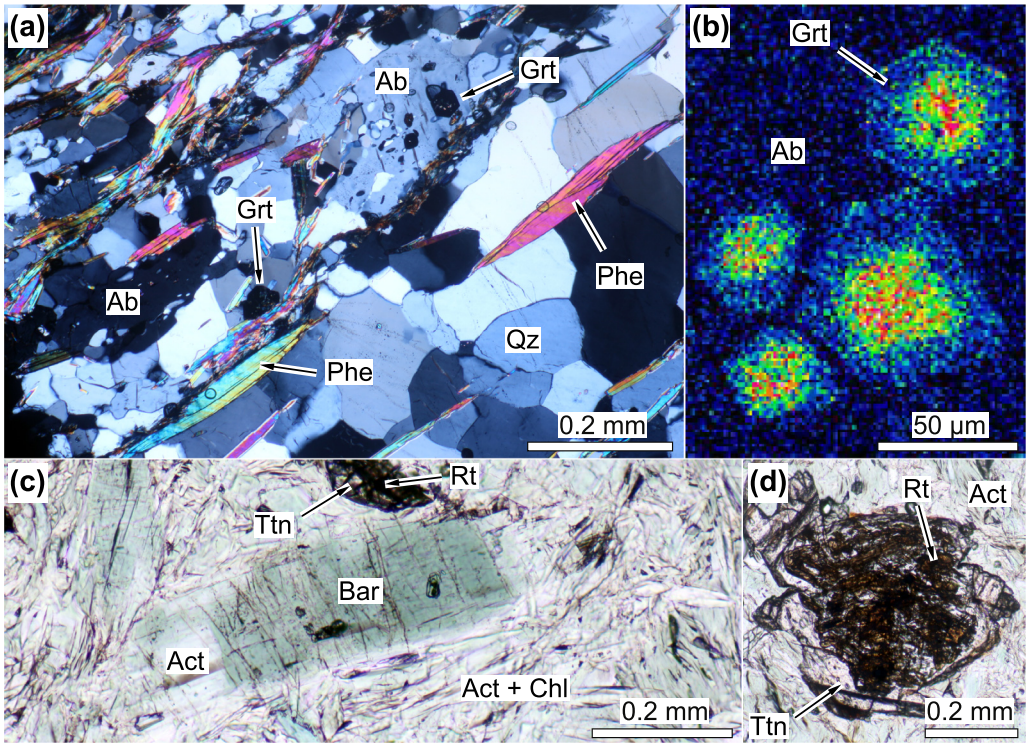

Fig. 2. Microphotographs showing the mineral assemblage of the collected samples. (a) Photomicrograph of the KMT08 pelitic schist, showing albite, garnet and phengite. (b) FE-SEM-EDS X-ray (Mn) image of small garnets in porphyroblastic albite. (c) Photomicrograph of the KTM11 mafic schist showing barroisite, titanite rutile and actinolite. (d) Photomicrograph showing the rutile replaced by titanite.

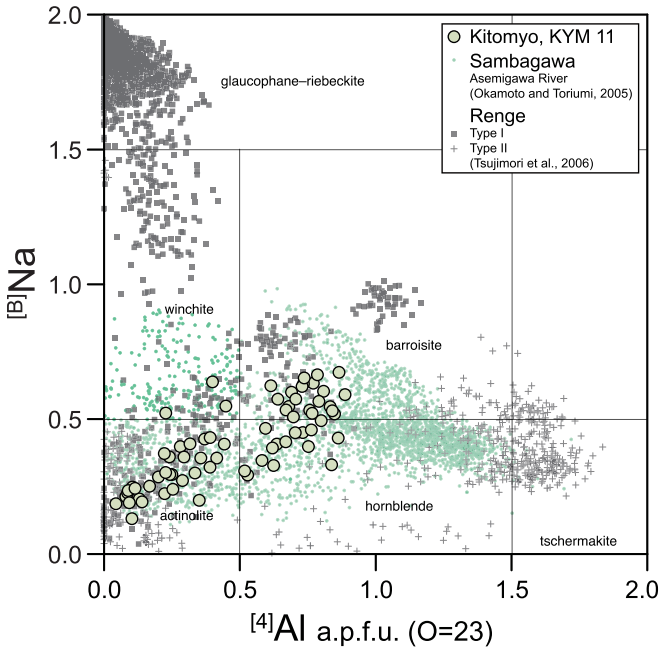

Fig. 3. [B]Na (Na in the B-site) versus [4]Al (Al in tetrahedral site) diagram for the subcalcic and calcic amphiboles of Kitomyo Schist (sample KTM11). For comparisons, subcalcic and calcic amphiboles of Sambagawa mafic schist (Okamoto & Toriumi, 2005) and sodic, subcalcic and calcic amphiboles of Renge metamorphic rocks (Tsujimori, Liou, Ernst, & Itaya, 2006) are also shown.

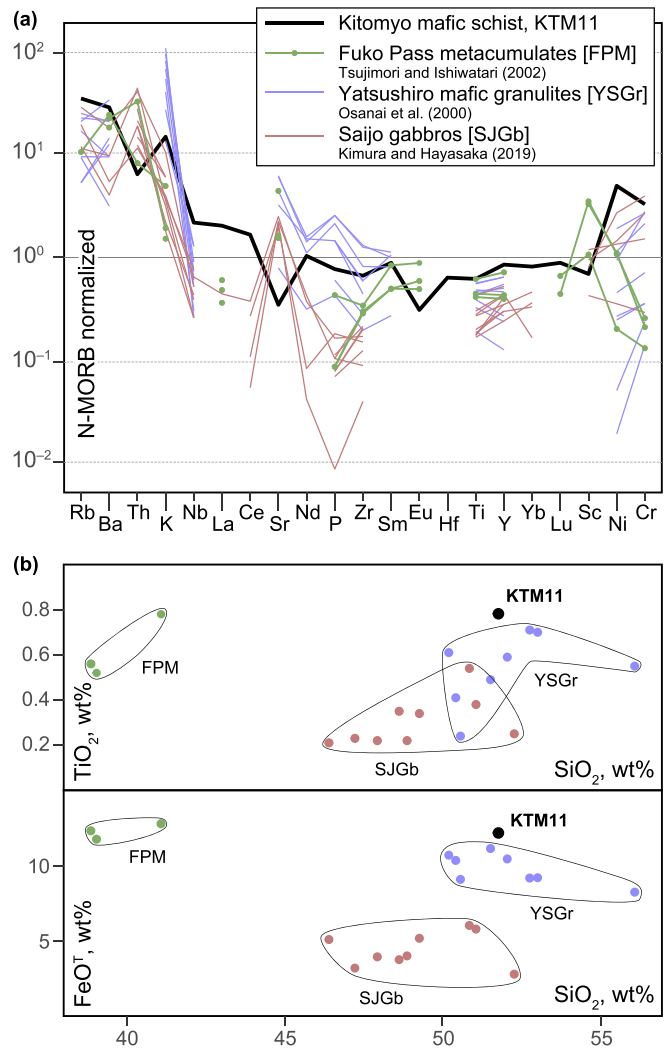

Fig. 4. Bulk-rock compositions of the KTM11 mafic schist sample of the Kitomyo Schist. For comparisons, Fuko Pass metacumulates [FPM] (Tsujimori & Ishiwatari, 2002), Yatsushiro mafic granulites [YSGr] of the Kurosegawa Belt (Osanai et al., 2014) and Saijo gabbros [SJGb] of the Oeyama Ophiolite (Kimura & Hayasaka, 2019) are also plotted. (a) N-MORB-normalized trace-element pattern. Normalizing values are from Sun and McDonough (1989), except Sc, Cr and Ni from Pearce (1982). (b) SiO_2 versus TiO_2 and FeO^T diagrams.

The sample KTM11 is characterized by somewhat peculiar bulk-rock composition (Table 2). It is quartz normative and shows moderate SiO_2 (51.8 wt%), low CaO (5.3 wt%) and Al_2O_3 (9.6 wt%), with MgO (11.3 wt %), FeO^T (12.2 wt%; total Fe as FeO), Na_2O (1.8 wt%), K_2O (1.09 wt%), TiO_2 (0.78 wt%); the loss of ignition was 4.7 wt%. The high MgO + FeO^T and Ni (450 $\mu g \cdot g^{-1}$), Cr (830 $\mu g \cdot g^{-1}$) and low CaO + Al_2O_3 and Sr (31 $\mu g \cdot g^{-1}$) (Table 2; Fig. 4) suggest that plagioclase-poor cumulate protolith; this is also supported by a clear negative Eu anomaly in N-MORB-normalized trace-element pattern (Fig. 4a). Comparing with geochemical features with Fuko Pass metacumulates (Tsujimori & Ishiwatari, 2002), gabbroic rocks of the Sanjo ultramafic body of the Oeyama Ophiolite (Kimura & Hayasaka, 2019), and Yatsushiro mafic granulites of the Kurosegawa Belt of Kyushu (Osanai et al., 2000) KTM11 has no similarity with those Early Paleozoic rocks, expecting a similar FeO^T and SiO_2 contents (Fig. 4b).

4.1.3. P–T condition of metamorphism

Pelitic schist KTM08 is characterized by a mineral assemblage of garnet + phengite + quartz + albite ± chlorite. The presence of garnet and the lack of biotite, oligoclase and paragonite indicate that the schist underwent a H*P* intermediate type metamorphism similar to apparent mineral assemblage of the garnet zone of the Sambagawa metamorphic belt (e.g., Aoki, Maruyama, Isozaki, Otoh, & Yanai, 2011; Itaya, Tsujimori, & Liou, 2011).

The *P–T* conditions for the H*P* intermediate type metamorphism characterized by the assemblage barroisite + epidote + rutile can be constrained through the use of phase equilibria. Based on the bulk-rock composition of KTM11, we modeled a *P–T* pseudosection (equilibrium phase diagram) using THERIAK-DOMINO software (de Capitani & Petrakakis, 2010) to evaluate quantitatively the *P–T* stability field of barroisitic amphibole. The pseudosection uses the thermodynamic dataset of Holland and Powell (1998); we adopted the solid solution models of minerals that used in Tsujimori and Ernst (2014). The calculated chemographic relations shows a *P–T* space of coexistence of barroisitic amphibole with epidote and rutile at P = ~0.8–1.5 GPa and T = 500–570 °C (Fig. 5a). Okamoto and Toriumi (2005) applied the Gibbs' method for subcalcic amphiboles in mafic schists of the Sambagawa Belt of Shikoku and estimated its *P–T* conditions. Using a new reference *P–T* condition for the Gibbs' method (Uno, Iwamori, & Toriumi, 2015), we calculated *P–T* conditions of amphiboles from the Kitomyo Schist and those from the Sambagawa Belt (Okamoto & Toriumi, 2005) (Fig. 5a). The *P–T* conditions based on the Gibbs' method for Kitomyo Schist overlaps with the *P–T* estimates of barroisitic amphiboles of Sambagawa mafic schist (Fig. 5a).

The observed retrograde assemblage fits those of a typical greenschist facies. The absence of biotite and high-Si phengite suggests P = ~0.6 GPa at T = 350 °C for the retrograde stage. The retrograde *P–T* path from epidote-amphibolite to greenschist facies (Fig. 5b) is relatively common in H*P* intermediate type metamorphic belt, such as Sambagawa Belt (Okamoto & Toriumi, 2005). Although the prograde *P–T* path could not be constrained in the Kitomyo Schist, the retrograde evolution suggests that the Kitomyo Schist had a cooling history similar to the coherent unit of the Sambagawa Belt, before it had trapped as a tectonic block. Such retrograde path is also common in some Renge

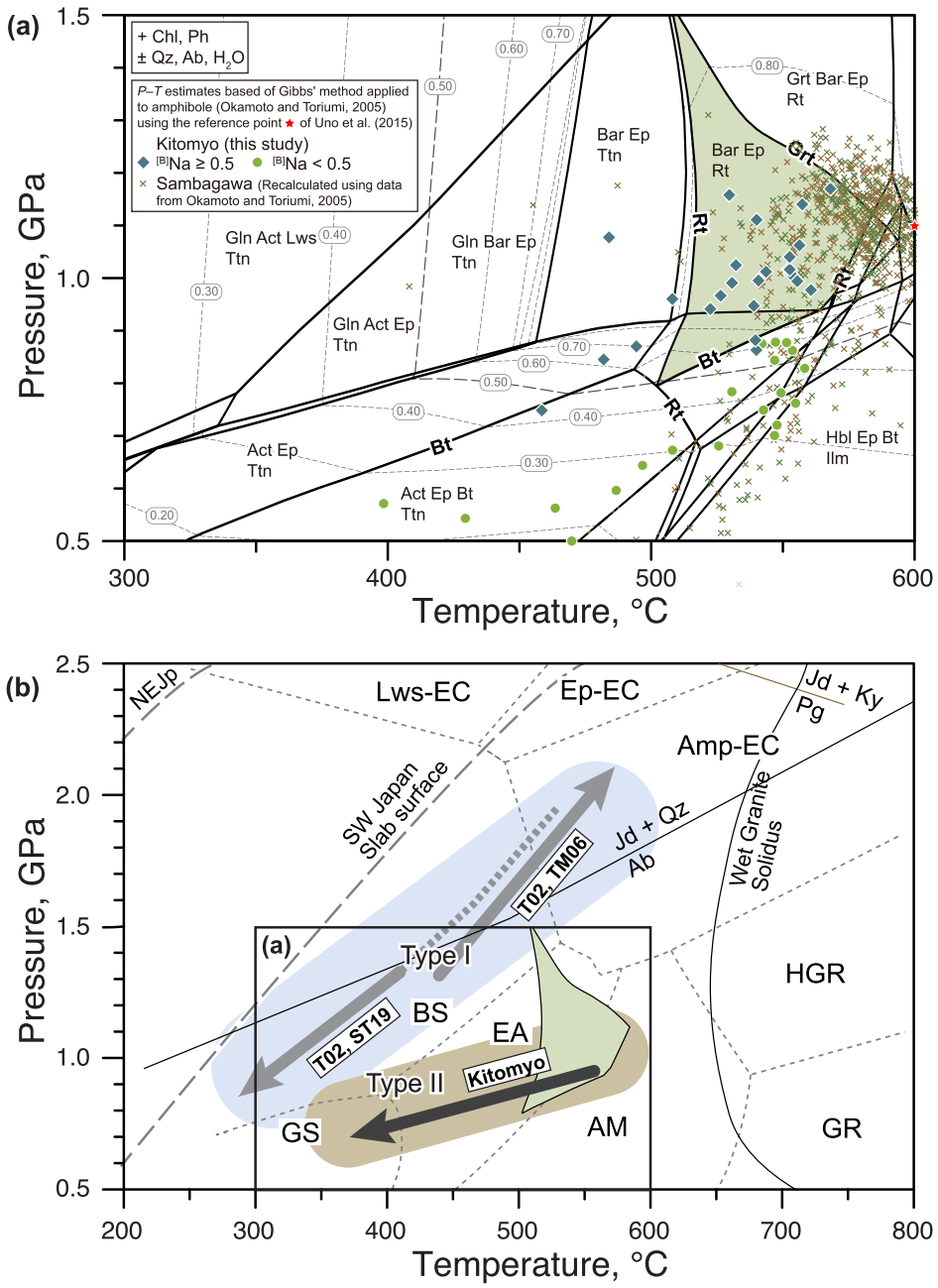

Fig. 5. (a) Equilibrium phase diagrams evaluating the stability field of KTM11 in greenschist–amphibolite facies. For comparisons, *P–T* estimates based on Gibb's method for barroisite and hornblende of Sambagawa schists by Okamoto and Toriumi (2005) are also plotted. (b) A *P–T* diagram showing a retrograde *P–T* path of the Kitomyo Schist (sample KTM11) and *P–T* fields for the inferred metamorphic condition of the Type I and Type II Renge metamorphic rocks (Tsujimori, 2010); prograde and retrograde *P–T* paths (grey arrows) are after Tsujimori (2010), Tsujimori and Matsumoto (2006), and Shinji and Tsujimori (2019).

metamorphic rocks (e.g., Kunugiza et al., 2017; Nakamizu, 1989). Tsujimori (2010) grouped such Renge Metamorphic Rocks as Type II, which do not contain glaucophane and differ from the *P–T* trajectories of glaucophane-bearing Type I blueschist and glaucophane-bearing eclogite). Petrological features of the Kitomyo Schist suggest similarity to the Type II Renge Metamorphic Rocks which do not contain glaucophane (Tsujimori, 2010).

4.2. Geochronology

Zircons (~60–150 μm) from the sample KTM08 have stubby and euhedral morphology and show internal CL texture. Most grains have thick cores exhibiting clear oscillatory zoning mantled by very thin overgrown rims (for example, grains L1, S2 and S5 of Fig. 6). The rims show high CL intensity. A few grains do not show obvious internal zoning (grain L2) and/or exhibits distinct highly-luminescent inherited core with mantled by faintly patchy dark-CL domain (grain S8). The zircon domains exhibiting oscillatory and strips of different CL intensity suggests magmatic origin. In contrast, thin rims with bright CL are characteristic for hydrothermal/metamorphic overgrowths (e.g., Aoki et al., 2020). Twelve zircon grains were analyzed using SHRIMP and LA-ICPMS after textural observations. The $^{206}Pb/^{238}U$ ages of oscillatory zoned zircons show a cluster at ~440 Ma (weighted mean 443 ± 2 Ma [MSWD = 1.92, n = 16]) and much older grains of Paleoproterozoic

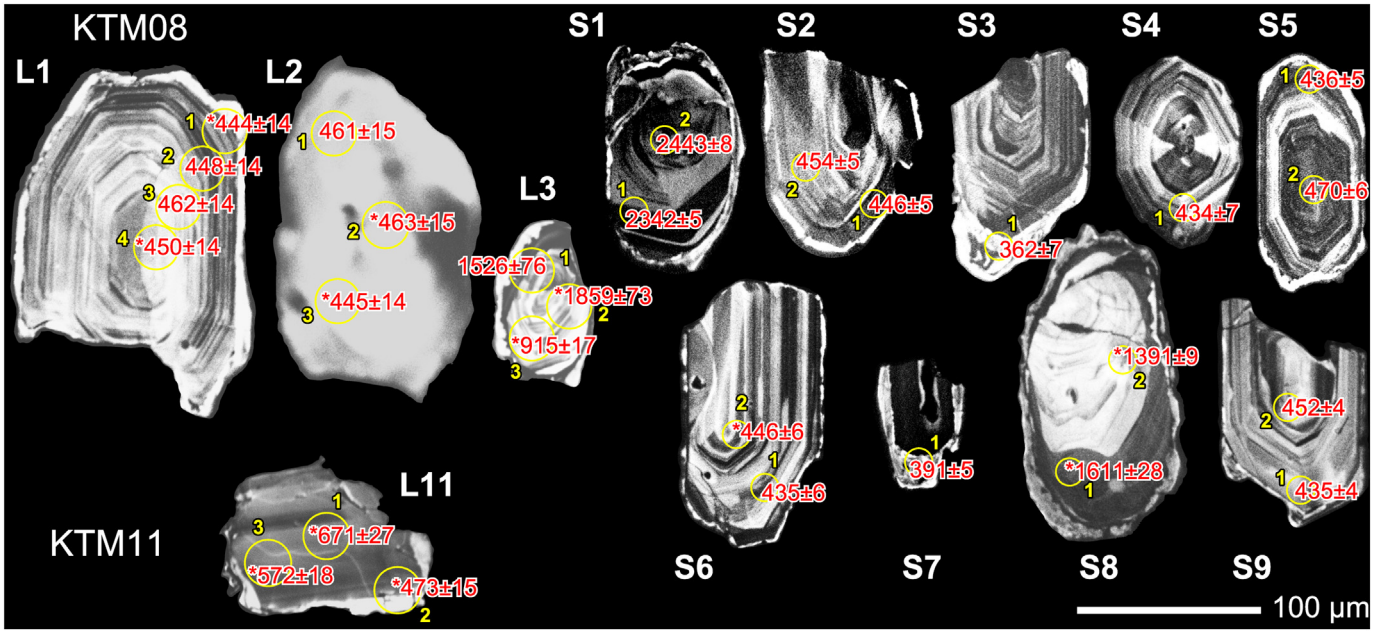

Fig. 6. Cathodoluminescence (CL) images of thirteen zircon grains separated from the Kitomyo Schists for LA-ICPMS and SHRIMP analyses. Circles indicate the laser ablation spots for the grains L1, L2, L3 and L11 and the ion beam spot for the grains from S1 to S9.

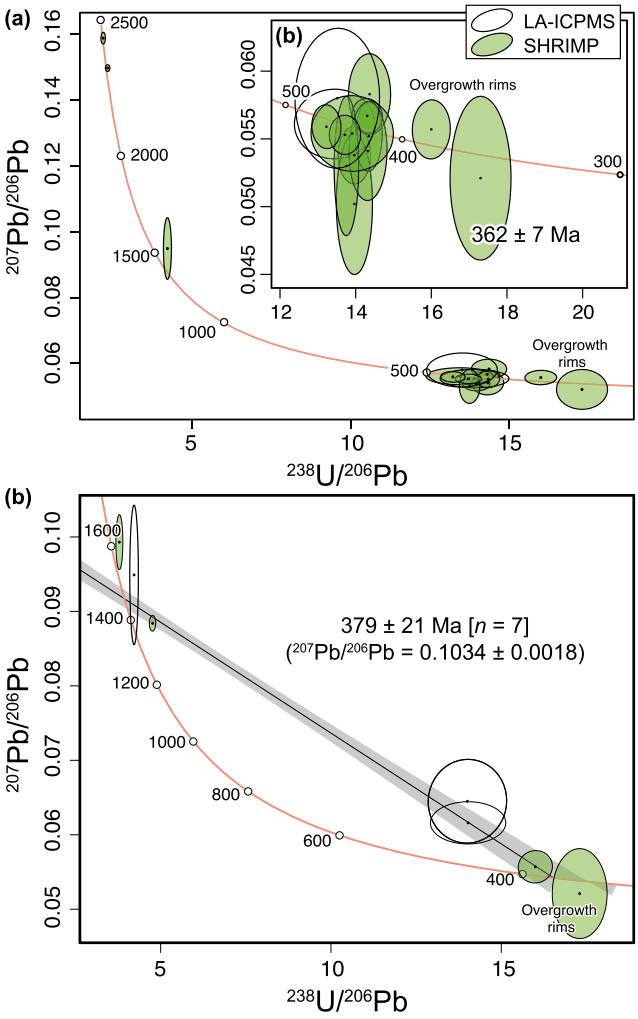

Fig. 7. (a) Tera-Wasserburg concordia diagram for concordant data of zircons form the Kitomyo Schist (sample KTM08). (b) Enlarged plots for a ~ 440 Ma cluster and two overgrowth rims. (c) Tera-Wasserburg concordia diagram showing an isochron line defined by discordant data between the two rim ages and a Mesoproterozoic ages.

($^{206}Pb/^{207}Pb$ ages of 2.44 Ga, 2.34 Ga and 1.86 Ga) and Mesoproterozoic age ($^{206}Pb/^{207}Pb$ age of 1.53 Ga) (Table 3, Fig. 7a). Relatively wide portion of two overgrowth rims (S3 and S7 of Fig. 6) were dated using SHRIMP. The rims yield $^{206}Pb/^{238}U$ age of 362 ± 7 and 391 ± 5 Ma (Table 3; Fig. 7). Since the later spot was overlapping partially to the mantle of grain, the timing of rim overgrowth should be younger than 391 Ma. If we consider discordant data between the two rim ages and a Mesoproterozoic age, the scattered trend defines an isochron line with a lower intercept at 379 ± 21 Ma [$n = 7$] (Fig. 7b).

We could separate only one zircon grain from the KTM11 mafic schist. The grain displays faintly planar banded zoning with a thin overgrown rim of bright luminescence (L11 of Fig. 6). Three spot analyses on the banded zoned domain did not show concordance. The apparent $^{206}Pb/^{238}U$ ages, 671 ± 27 Ma, 572 ± 18 Ma, 473 ± 15 Ma (Table 3), may suggest Early Paleozoic formation of the protolith.

New phengite K–Ar age was shown in Table 4. It is noteworthy that the new data, 400.2 ± 7.9 Ma, for phengite separates (8.139 ± 0.16 wt % K) overlaps the previous ages reported by Maruyama and Ueda (1975) and significantly older than the zircon rim ages.

5. Discussion

5.1. Significance within the 'proto-Japan' scenario

The geological nature of Early Paleozoic subduction zone metamorphism in proto-Japan is poorly understood due to the paucity of Early Paleozoic H*P* metamorphic rocks with robust evidence of 'cold' paleogeotherm. The occurrence of jadeitite associated with serpentinite derived from the Paleozoic ophiolite and serpentinite mélange of the Hida-Gaien and the Oeyama Belt suggests an Early Paleozoic subduction initiation (Tsujimori, 2017; Tsujimori & Harlow, 2017). Early Paleozoic kyanite- and paragonite-bearing metacumulates (Tsujimori et al., 2000; Tsujimori & Liou, 2004) also support Early Paleozoic subduction zone metamorphism. On the other hand, no Early Paleozoic blueschist-facies mineral assemblage has been confirmed yet (Ichiyama, Koshiba, Ito, & Tamura, 2020; Tsujimori, 2010; Tsujimori & Itaya, 1999; Tsujimori & Liou, 2004).

Does the Kitomyo Schist provide a clue for the first generation of subduction zone along the 'proto-Japan'? The youngest detrital zircons in metasedimentary rocks of Pacific-type H*P* belt can constrain the maximum depositional age of trench-fill sediments (e.g., Aoki et al., 2011). Our zircon geochronology found its youngest cluster of detrital zircons at ~440 Ma. Early Paleozoic calc-alkaline granitoids with zircon U–Pb ages of ~445–435 Ma are sporadically found as blocks in the Kurosegawa Belt (e.g., Aitchison, Hada, Ireland, & Yoshikura, 1996; Aoki et al., 2015). Recently, a wide distribution of the Early Paleozoic calc-alkaline granitoids has been confirmed in the Cathaysia Block of the South China Craton (e.g., Liu et al., 2014; Ou et al., 2019; Shu et al., 2014; Wang et al., 2011). In the Kurosegawa Belt of Kyushu, a small exposure of garnet-bearing granulite and amphibolite yield zircon U–Pb ages of 453–440 Ma (Osanai et al., 2014). These calc-alkaline magmatic activities and granulite-facies metamorphic rocks would have formed

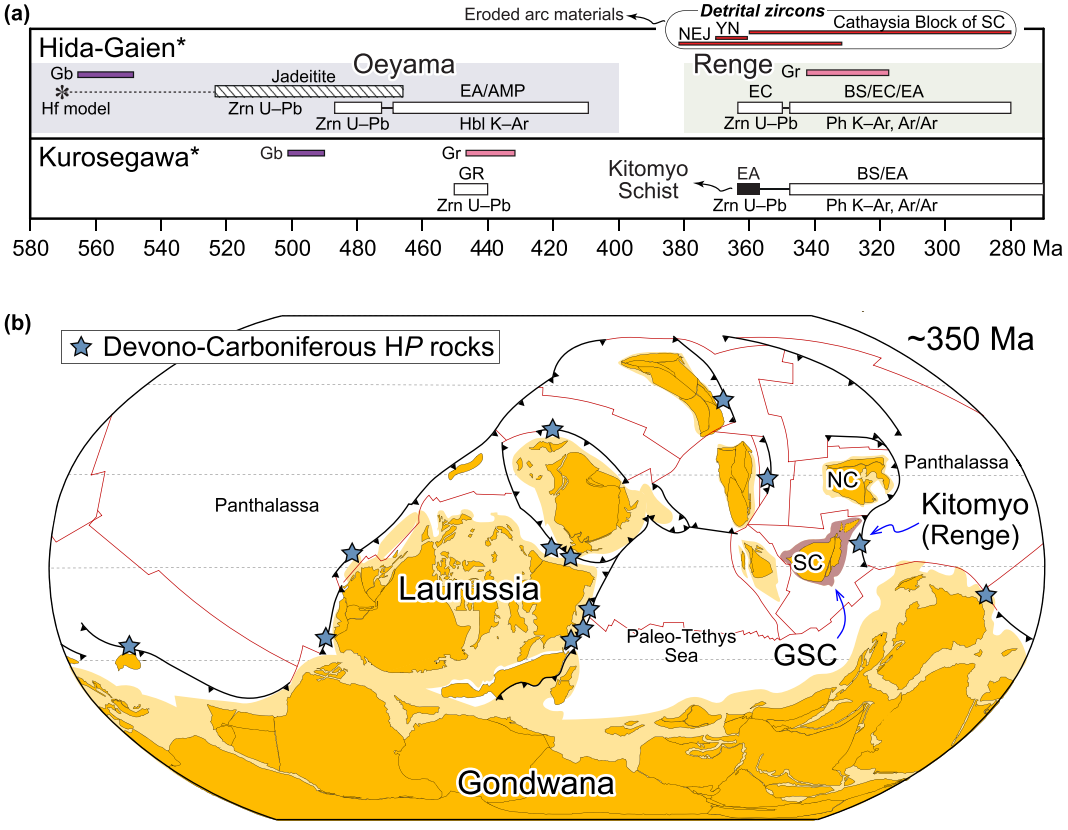

Fig. 8. (a)_Summary of geochronological data for metamorphic/ metasomatic and igneous rocks from the Hida-Gaien, Oeyama, Renge and Kurosegawa Belts of Japan (modified after Tsujimori & Harlow, 2012 and Tsujimori, 2017); additional data includes Ichiyama et al. (2020) and Yoshida et al. (2020). Names with '*' represent composite geotectonic units. Age ranges of Late Paleozoic detrital zircons from sedimentary (and metasedimentary) rocks from the Cathaysia Block of South China Craton [SC] (Hu et al., 2012), the Yeongnam Massif [YN] (Cheong et al., 2015), Northeast Japan [NEJ] (Isozaki et al., 2014) are also shown. Abbreviations of minerals, rocks, and metamorphic facies: Zrn, zircon; PhPh, phengite; Hbl, hornblendic amphibole; Gb: gabbroic rocks; Gr, granitic rocks; BS, blueschist facies; EA, epidote-amphibolite facies; EC, eclogite facies, AM, amphibolite facies; GR, granulite facies. (b) Early Carboniferous plate reconstruction showing the location of South China (SC) and North China [NC] Cratons (modified after Young et al., 2019), 'Greater South China' (Isozaki, 2019) and the Kitomyo Schist (Kitomyo). Note that the location of the Paleozoic Japanese arc has been also suggested in paleogeographical reconstructions by Cocks and Cocks and Torsvik, 2012. Major localities of high-pressure metamorphic rocks (Tsujimori & Ernst, 2014) are also shown.

concomitantly to the first generation of 'proto-Japan' arc crust (e.g., Isozaki, 2019). Considering regional geological context, we postulated that ~445–435 Ma granites formed part of the arc-crust source for the ~440 Ma detrital zircons in pelitic schist of the Kitomyo Schist. The ~1.5 Ga, ~1.8 Ga and ~ 2.4 Ga detrital grains in KTM08 might have derived from the cratonic blocks or inherited grains of the ~445–435 Ma arc crust.

Determining metamorphic ages using zircons in low-temperature metamorphic rocks is always challenging due to the limited zircon growth under such conditions (e.g., Hay & Dempster, 2009). As our case has shown, metamorphic overgrowths are volumetrically too small for analyses. However successful spot analyses revealed the timing of metamorphic overgrowths as young as ~360 Ma (Fig. 8). Considering the inferred *P–T* trajectory of the Kitomyo Schist, metamorphic zircon overgrowth can be expected at the peak epidote-amphibolite condition rather than greenschist-facies overprinting. We interpret the rims ages represent a timing of epidote-amphibolite facies metamorphism of the Kitomyo Schist, in which the assemblage barroisitic amphibolite + rutile was stable. The ~360 Ma H*P* intermediate-type metamorphism is coeval with the timing of H*P* metamorphism of the Renge Metamorphic Rocks as defined by zircon U–Pb ages (Tsujimori, 2010; Yoshida, Taguchi, Ueda, Horie, & Satish-Kumar, 2020). Then why the age is significantly younger than new phengite K–Ar age?

K–Ar system dating (including Ar/Ar) has been routinely used to determine the cooling ages of H*P* metamorphic rocks. However, it has been also known chronological discrepancy due to the excess ^{40}Ar trapped in white micas (e.g., Itaya et al., 2011; Itaya & Tsujimori, 2015). Phengite K–Ar ages significantly older than zircon U–Pb ages have been well known in the eclogite-facies meta sedimentary rocks associated with meta-peridotite in the Sambagawa Belt (Itaya & Tsujimori, 2015). An older Cr-bearing phengite K–Ar age was also confirmed in metasomatized ultramafic rocks of the Renge Belt (Tsujimori & Itaya, 1999). Considering mantle materials have extreme $^{40}Ar/^{36}Ar$ ratio (e.g. Kaneoka & Takaoka, 1980), it is highly possible that the significantly older phengite age is due to excess ^{40}Ar derived from the surrounding ultramafic rocks (e.g., Itaya & Tsujimori, 2015). Another possibility would be the detrital origin of white mica. If the closure temperature is high as ~600 °C (e.g., Gozu, Yagi, Thanh, Itaya, & Compagnoni, 2016; Itaya, 2020), the presence of older detrital mica can result in the old age. However, moderate to high-Si feature (3.3–3.6 a.p.f.u.) of the phengite of the Kitomyo Schist exclude the possibility.

Recently Yang, Santosh, Maruyama, and Nakagawa (2016) and Hu et al. (2017) conducted zircon U–Pb geochronology of blueschist, rodingites and host serpentinites in the Kurosegawa Belt near Kochi City. Yang et al. (2016) found 505 ± 3 Ma and 503 ± 3 Ma magmatic zircons inherited in a low-grade blueschist; Osanai et al. (2014) has also dated magmatic zircons inherited in a Late Paleozoic blueschist-facies metagabbro and found 493 ± 4.9 Ma. Hu et al. (2017) found a wide age range from 51 Ma to 1.58 Ga in rodingite samples: 197 ± 5 Ma ($n = 5$), 262 ± 2 Ma ($n = 4$), 278 ± 9 Ma ($n = 3$), 294 ± 6 Ma ($n = 2$), 315 ± 11 Ma ($n = 3$), 811 ± 11 Ma (n = 4). They also confirmed a wide age range from 62 Ma to 2.53 Ga with clusters of 379 ± 15 Ma

Table 1
Rappresentative SEM–EDS analyses for the Kitomyo Schist. Abbreviation: Grt, garnet; Ph, phengite; Ep, epidote; Bar, barroisitic amphibole; Chl, chlorite.

	KTM08				KTM11						
	Grt (rim)	Grt (core)	Ph	Ep	Bar	Bar	Act	Act	Ep	Chl	Ph
SiO_2	37.57	37.61	49.49	38.23	50.71	51.92	53.13	54.64	37.05	28.11	53.91
TiO_2	0.09	0.27	0.35	0.16	0.11		0.21		0.01	0.88	0.07
Al_2O_3	20.27	20.5	26.95	25.4	6.68	6.87	2.70	1.07	22.13	17.87	21.85
Cr_2O_3			0.13	0.06	0.22	0.32	0.31	0.47	0.10	0.18	0.39
$Fe_2O_3^T$				10.97					15.80		
FeO^T	30.19	18.70	4.26		17.69	15.82	11.87	10.81		20.39	4.69
MnO	1.39	11.53		0.42	0.20	0.41	0.50	0.35	0.48	0.33	
MgO	1.30	0.66	2.82	0.08	12.48	12.78	15.91	16.20		19.93	4.92
CaO	8.51	10.76	0.09	23.09	8.8	9.19	10.86	11.21	21.89	0.31	0.03
Na_2O			0.69	0.12	3.11	2.79	1.16	0.75			0.01
K_2O			10.25	0.06	0.18	0.12	0.16	0.16			10.64
Total	99.32	100.03	95.03	98.59	100.18	100.22	96.81	95.66	97.46	88.00	96.51
O=	12	12	11	12.5	23	23	23	23	12.5	28	11
Si	3.034	3.013	3.353	2.997	7.134	7.266	7.608	7.914	2.987	5.757	3.592
Ti	0.005	0.016	0.018	0.009	0.012	0.000	0.023	0.000	0.001	0.136	0.004
Al	1.929	1.936	2.152	2.347	1.108	1.133	0.456	0.183	2.103	4.313	1.716
Cr	0.000	0.000	0.007	0.004	0.024	0.035	0.035	0.054	0.006	0.029	0.021
Fe^{3+}				0.647	1.043	0.766	0.564	0.217	0.959		
Fe^{2+}	2.039	1.253	0.241		1.038	1.085	0.857	1.092		3.492	0.261
Mn	0.095	0.782	0.000	0.028	0.024	0.049	0.061	0.043	0.033	0.057	0.000
Mg	0.156	0.079	0.285	0.009	2.617	2.666	3.396	3.498	0.000	6.084	0.489
Ca	0.736	0.924	0.007	1.940	1.326	1.378	1.666	1.740	1.891	0.068	0.002
Na	0.000	0.000	0.091	0.018	0.848	0.757	0.322	0.211	0.000	0.000	0.001
K	0.000	0.000	0.886	0.006	0.032	0.021	0.029	0.030	0.000	0.000	0.904
Total	7.996	8.003	7.038	8.006	15.207	15.156	15.017	14.980	7.979	19.936	6.989
$^{[B]}Na$					0.67	0.62	0.33	0.26			
Mg#	0.07	0.06	0.54		0.72	0.71	0.80	0.76		0.64	0.65
X_{alm}	0.67	0.41									
$X_{sps}s_{ps}$	0.03	0.26									
X_{grs}	0.24	0.30									
X_{pyr}	0.05	0.03									

$Fe_2O_3^T$ = total Fe as Fe_2O_3; FeO^T = total Fe as FeO
Mg# = Mg/(Mg + Fe^{2+}) atomic ratio

Table 2
Bulk-rock major- and trace-element concentrations of the sample KTM11.

wt%	
SiO_2	51.75
TiO_2	0.78
Al_2O_3	9.63
FeO^T	12.17
MnO	0.24
MgO	11.30
CaO	5.27
Na_2O	1.81
K_2O	1.09
P_2O_5	0.09
LOI	4.73
Total	98.86
$\mu g \cdot g^{-1}$	
Rb	20
Ba	184
Th	0.78
U	0.29
Nb	5.1
Ta	0.36
La	5.7
Ce	12.5
Pr	1.68
Sr	31
Nd	7.55
Zr	49
Hf	1.3
Sm	2.33
Eu	0.313
Gd	3.35
Tb	0.59
Dy	3.87
Ho	0.86
Y	23.8
Er	2.59
Tm	0.376
Yb	2.48
Lu	0.403
Ni	450
Sc	28
Cr	830

($n = 10$), 467 ± 3 Ma ($n = 5$) and 488 ± 3 Ma ($n = 10$) in a serpentinite sample. Although the presence of Mesozoic to Paleogene zircons in the serpentinite of Paleozoic geotectonic unit suggests multiple hydrothermal zircon growth in serpentinite and/or neotectonic mingling of the serpentinite and younger strata. Probably more detailed zircon geochronology for the mélange-matrix serpentinite is required than that documented in previous studies. Nevertheless, some Late Paleozoic zircons might have related to the Late Paleozoic subduction zone metamorphism that is recorded in the Renge Metamorphic Rocks and their equivalents in the Kurosegawa Belt (Fig. 8a).

5.2. Tectonic implications for East Asia

Where does the late Paleozoic oceanic subduction zone correlate with petrotectonic units in East Asia? Ernst, Tsujimori, Zhang, and Liou (2007) has considered the Permo-Triassic Tongbai–Dabie–Sulu-Imjingang–Gyeonggi–Renge–Suo–Sikhote-Alin Orogenic Belt along the paleo-Pacific edge of cratonic Asia. The orogen is characterized by the multiple events involving accretion of outboard oceanic arcs + microcontinental fragments against the East Asian margin at ~320–210 Ma, including the deeply subducted sector like the Sulu–Dabie ultrahigh-pressure Belt. However, during the last decade growing evidence supports the 'proto-Japan' plate convergence at the eastern margin of the Cathaysia Blocks of the South China Craton (e.g., Cocks and Cocks and Torsvik, 2012; Isozaki, Aoki, Sakata, & Hirata, 2014; Isozaki et al., 2017; Isozaki, 2019) (Fig. 8b). Recent zircon geochronology re-approved the classic idea of Isozaki (1997) that the 'proto-Japan' was formed at an oceanic subduction zone between the paleo Pacific plate and South China Craton. Moreover Isozaki (2019) has proposed the 'Greater South China'; this would consist of an amalgamated continental block that extended from the Yangtze plus Cathaysia Blocks of the South China Craton, passing through Korean Peninsula to the Bureya, Jiamusi, and Khanka Blocks of Sikhote-Alin (Primorye, Russia). However, the exposure of the Late Paleozoic H*P* metamorphic rocks (Renge metamorphic rocks and their equivalents) with ~360–280 Ma is limited only to Japan, and their eastern or western counterparts are missing in either Cathaysia or Sikhote-Alin. So far, all described blueschists in Sikhote-Alin are younger (~250 Ma) and rather similar to Suo Belt (Ishiwatari & Tsujimori, 2003). Similarly, Devono–Carboniferous batholiths do not crop out in the eastern margin of the 'Greater South China'. However, there are abundant ~360–280 Ma detrital zircons in Permian and Jurassic sedimentary rocks in eastern part of the Cathaysia Block (Hu et al., 2012) and ~ 380–340 Ma detrital zircons in Permian sedimentary rocks in NE Japan (Isozaki et al., 2014). Devonian population (~370 Ma) of detrital zircons are also known in metasedimentary rocks of the Yeongnam Massif (Cheong, Kim, Kim, & Cho, 2015). These detrital signatures suggest a relatively extensive region of granitic magmatism existed along the 'Great South China' margin and was subsequently eroded. Considering the information together with regional geological context, geological evidence of a mature arc–trench system during Late Paleozoic oceanic subduction is widely recorded as detrital zircons. This also suggest that during late Devonian-early Carboniferous the Greater South China terrane likely developed a paired belt (c.f. Sanbagawa Belt and Ryoke Bet (including granitic batholiths): Miyashiro, 1961; Brown, 2010). The surface erosion and further tectonic events probably erased the Devono–Carboniferous batholith belt that was paired with the Late Paleozoic H*P* metamorphic rocks, such as the Kitomyo Schist.

6. Conclusion

Reappraisal of the oldest high-pressure type schist in Japan confirmed that the Kitomyo Schist of the Kurosegawa Belt found that the schist is characterized by the H*P* intermediate-type, epidote-amphibolite facies metamorphism. The retrograde *P–T* path suggests that the Kitomyo Schist had a cooling history similar to the coherent unit of the Sambagawa Belt, before trapping as a tectonic block. The Kitomyo Schist contains ~440 Ma detrital magmatic zircon with very thin overgrown rims of ~360 Ma. Therefore, the schist is not the oldest H*P* type schist in Japan and rather comparable to the Late Paleozoic Renge Metamorphic Rocks and their equivalents in the Kurosegawa Belt. The both Kitomyo Schist and the Renge Metamorphic Rocks formed at the oceanic subduction zone along the 'Greater South China' margin.

Table 1 Representative SEM–EDS analyses of the major constituent minerals in the Kitomyo Schist. Abbreviation: Grt, garnet; Ph, phengite; Ep, epidote; Bar, barroisitic amphibole; Chl, chlorite.

Declaration of Competing Interest

The authors declare that they have no known competing financial interests or personal relationships that could have appeared to influence the work reported in this paper.

Acknowledgments

This research was supported by CNEAS and FRIS of Tohoku University in part by grants from the MEXT/JSPS KAKENHI JP15H05212 and JP18H01299 to TT and JP16F16329 to TT and DPG. This was also supported by MEXT Private University Research Branding Project (Okayama University of Science) and MEXT/JSPS KAKENHI JP19K04043 to KA. We

Table 3
Zircon U–Pb isotopic data of zircons from the Kitomyo Schist (KTM08 and KTM11). Spot IDs with 'L' represent LA-ICPMS data, and with 'S' represent SHRIMP data. Spot IDs with '*' represent discordant data. In SHRIMP data, common Pb was corrected using measured ^{204}Pb.

Spot ID	^{207}Pb/^{235}U	2σ	^{206}Pb/^{238}U	2σ	^{207}Pb/^{206}Pb	2σ	^{207}Pb/^{235}U age	2σ	^{206}Pb/^{238}U age	2σ	^{207}Pb/^{206}Pb age	2σ	U, μg/g	Th, μg/g	^{232}Th/^{238}U
LA-ICPMS															
L1#1*	0.606	0.0226	0.0713	0.00230	0.0616	0.00116	481.2	14	444.2	14	661.8	40	244	79.9	0.33
L1#2	0.549	0.0210	0.0719	0.00232	0.0554	0.00114	444.5	14	447.7	14	428.3	46	204	81.3	0.40
L1#3	0.575	0.0214	0.0744	0.00239	0.0561	0.00105	461.5	14	462.4	14	457.3	41	263	98.8	0.38
L1#4*	1.29	0.0465	0.0723	0.00233	0.130	0.00208	842.3	21	449.9	14	2094	28	208	81.5	0.39
L2#1	0.592	0.0291	0.0740	0.00245	0.0580	0.00211	472.0	19	460.5	15	528.5	80	49.0	15.1	0.31
L2#2*	1.02	0.0450	0.0744	0.00246	0.0995	0.00290	714.0	23	462.6	15	1614	54	48.1	14.5	0.30
L2#3*	0.635	0.0309	0.0714	0.00236	0.0645	0.00230	499.4	19	444.8	14	758.5	75	48.2	13.3	0.28
L3#1	3.10	0.130	0.237	0.00288	0.0949	0.00383	1432	32	1369	15	1526	76	453	127	0.28
L3#2*	3.95	0.166	0.252	0.00308	0.114	0.00459	1624	34	1448	16	1859	73	349	150	0.43
L3#3*	0.768	0.107	0.153	0.00305	0.0365	0.00503	578.7	61	915.2	17			7.23	0.932	0.13
L11#1*	1.29	0.080	0.110	0.00460	0.0851	0.00392	840.0	36	670.8	27	1318	89	14.8	10.5	0.71
L11#2*	0.643	0.0280	0.0762	0.00250	0.0613	0.00177	504.4	17	473.2	15	648.6	62	76.2	43.0	0.56
L11#3*	0.847	0.0441	0.0927	0.00310	0.0663	0.00265	623.3	24	571.5	18	815.9	83	28.4	26.4	0.93
SHRIMP															
S1#1	8.85	0.2239	0.4288	0.01058	0.1497	0.00084	2323	12	2300	24	2342	4.8	846	51.9	0.061
S1#2	9.99	0.2759	0.4562	0.01191	0.1588	0.00143	2434	13	2423	26	2443	7.6	276	136	0.49
S2#1	0.532	0.0218	0.0716	0.00180	0.0538	0.00175	433.0	7.2	446	5.4	364.6	37	450	275	0.61
S2#2	0.556	0.0182	0.0729	0.00181	0.0553	0.00118	449.1	5.9	453.8	5.4	425.1	24	551	532	0.97
S3#1	0.415	0.0425	0.0578	0.00220	0.0521	0.00495	352.5	15	362.0	6.7	290.3	109	196	86.9	0.44
S4#1	0.559	0.0294	0.0696	0.00220	0.0583	0.00244	451.1	10	433.6	6.6	541.8	46	694	307	0.44
S5#1	0.547	0.0166	0.0699	0.00170	0.0567	0.00104	442.8	5.5	435.6	5.1	480.1	20	1051	552	0.52
S5#2	0.583	0.0200	0.0756	0.00188	0.0559	0.00132	466.4	6.4	470.0	5.6	448.5	26	581	281	0.48
S6#1	0.521	0.0320	0.0698	0.00193	0.0541	0.00297	425.7	11	435.0	5.8	375.5	62	162	76.4	0.47
S6#2*	0.496	0.0443	0.0716	0.00200	0.0502	0.00427	408.9	15	446.1	6.0	204.4	99	170	152	0.89
S7#1	0.480	0.0194	0.0625	0.00153	0.0557	0.00178	398.1	6.6	390.6	4.7	441.8	36	824	608	0.74
S8#1*	3.608	0.1351	0.264	0.00574	0.0993	0.00302	1551	15	1508	15	1611	28	132	81.5	0.62
S8#2*	2.561	0.0478	0.210	0.00336	0.0884	0.00085	1290	6.8	1230	9.0	1391	9.2	118	34.9	0.30
S9#1	0.531	0.0227	0.0697	0.00132	0.0552	0.00212	432.3	7.5	434.6	4.0	419.8	43	99.9	54.4	0.54
S9#2	0.531	0.0433	0.0727	0.00143	0.0530	0.00419	432.6	14	452.2	4.3	329.8	90	464	143	0.31

Table 4
Phengite K–Ar age of pelitic schist (KTM08) of the Kitomyo Schist.

	K, wt%	Rad. ^{40}Ar, 10^{-8} cc STP/g	K–Ar age, Ma	Non-rad. ^{40}Ar, %
KTM08 phnegite	8.139 ± 0.163	14,140.7 ± 134.5	400.2 ± 7.9	0.6

thank constructive comments from Tadao Nishiyama, Tetsumaru Itaya and an anonymous reviewer. We extend our appreciation to Atsushi Okamoto for his guidance on the Gibbs' method for amphiboles.

References

Aitchison, J.C., Hada, S., Ireland, T., Yoshikura, S., 1996. Ages of Silurian radiolarians from the Kurosegawa terrane, Southwest Japan constrained by U/Pb SHRIMP data. Journal of Southeast Asian Earth Sciences 14 (1–2), 53–70. https://doi.org/10.1016/S0743-9547(96)00045-1.

Aoki, K., Isozaki, Y., Yamamoto, A., Sakata, S., Hirata, T., 2015. Mid-Paleozoic arc granitoids in SW Japan with Neoproterozoic xenocrysts from South China: New zircon U–Pb ages by LA-ICP-MS. J. Asian Earth Sci. 97, 125–135. https://doi.org/10.1016/j.jseaes.2014.10.018.

Aoki, K., Maruyama, S., Isozaki, Y., Otoh, S., Yanai, S., 2011. Recognition of the Shimanto HP metamorphic belt within the traditional Sanbagawa HP metamorphic belt: new perspectives of the Cretaceous-Paleogene tectonics in Japan. J. Asian Earth Sci. 42, 355–369. https://doi.org/10.1016/10.1016/j.jseaes.2011.05.001.

Aoki, S., Aoki, K., Tsuchiya, Y., Kato, D., 2019. Constraint on the eclogite age of the Sanbagawa metamorphic rocks in Central Shikoku, Japan. International Geology Review 61 (18), 2211–2226. https://doi.org/10.1080/00206814.2019.1581997.

Aoki, S., Aoki, K., Tsujimori, T., Sakata, S., Tsuchiya, Y., 2020. Oceanic-arc subduction, stagnation, and exhumation: zircon U–Pb geochronology and trace-element geochemistry of the Sanbagawa eclogites in Central Shikoku, SW Japan. Lithos 358-359, 105378. https://doi.org/10.1016/j.lithos.2020.105378.

Brown, M., 2010. Paired metamorphic belts revisited. Gondw. Res. 18 (1), 46–59. https://doi.org/10.1016/j.gr.2009.11.004.

Cocks, L.R.M, Torsvik, T.H, 2012. The dynamic evolution of the Palaeozoic geography of eastern Asia. Earth-Science Reviews 117, 40–79. https://doi.org/10.1016/j.earscirev.2012.12.001.

de Capitani, C., Petrakakis, K., 2010. The computation of equilibrium assemblage diagrams with Theriak/Domino software. Am. Mineral. 95, 1006–1016. https://doi.org/10.2138/am.2010.3354.

Cheong, C.S., Kim, N., Kim, J., Cho, M., 2015. The Silurian-Devonian magmatism recorded in detrital zircons from the Andong area, northeastern Yeongnam Massif, Korea. Geosciences Journal 19 (3), 393–405. https://doi.org/10.1007/s12303-014-0060-4.

Ernst, W.G., Tsujimori, T., Zhang, R., Liou, J.G., 2007. Permo-Triassic collision, subduction-zone metamorphism, and tectonic exhumation along the East Asian continental margin. Annu. Rev. Earth Planet. Sci. 35, 73–110. https://doi.org/10.1146/annurev.earth.35.031306.140146.

Gozu, C., Yagi, K., Thanh, N.X., Itaya, T., Compagnoni, R., 2016. White mica K-Ar geochronology of HP-UHP units in the Lago di Cignana area, western Alps, Italy: Tectonic implications for exhumation. Lithos 248-251, 109–118. https://doi.org/10.1016/j.lithos.2016.01.015.

Hada, S., Ishii, K.I., Landis, C.A., Aitchison, J., Yoshikura, S., 2001. Kurosegawa Terrane in Southwest Japan: Disrupted remnants of a Gondwana-derived terrane. Gondw. Res. 4 (1), 27–38. https://doi.org/10.1016/S1342-937X(05)70652-3.

Hay, D.C., Dempster, T.J., 2009. Zircon behaviour during low-temperature metamorphism. J. Petrol. 50 (4), 571–589. https://doi.org/10.1093/petrology/egp011.

Holland, T.J.B., Powell, R., 1998. An internally consistent thermodynamic data set for phases of petrological interest. J. Metam. Geol. 16, 309–343. https://doi.org/10.1111/j.1525-1314.1998.00140.x.

Hosotani, H., Banno, S., 1986. Amphibole composition as an indicator of subtle grade variation in epidote-glaucophane schists. J. Metam. Geol. 4 (1), 23–35. https://doi.org/10.1111/j.1525-1314.1986.tb00336.x.

Hu, C.N., Santosh, M., Yang, Q.Y., Kim, S.W., Nakagawa, M., Maruyama, S., 2017. Magmatic and metasomatic imprints in a long-lasting subduction zone: evidence from zircon in rodingite and serpentinite of Kochi, SW Japan. Lithos 274-275, 349–362. https://doi.org/10.1016/j.lithos.2017.01.008.

Hu, X., Huang, Z., Wang, J., Yu, J., Xu, K., Jansa, L., Hu, W., 2012. Geology of the Fuding inlier in southeastern China: Implication for late Paleozoic Cathaysian paleogeography. Gondw. Res. 22 (2), 507–518.

Ichiyama, Y., Koshiba, T., Ito, H., Tamura, A., 2020. Geochemistry and magmatic zircon U–Pb dating of amphibolite blocks in the Omi serpentinite mélange, north Central Japan: possible subduction of the Cambrian oceanic crust. J. Mineral. Petrol. Sci. 115 (4), 313–321. https://doi.org/10.2465/jmps.191205.

Ishiwatari, A., Tsujimori, T., 2003. Paleozoic ophiolites and blueschists in Japan and Russian Primorye in the tectonic framework of East Asia: a synthesis. Island Arc 12 (2), 190–206. https://doi.org/10.1046/j.1440-1738.2003.00390.x.

Isozaki, Y., 1997. Contrasting two types of orogen in Permo-Triassic Japan: Accretionary versus collisional. Island Arc 6 (1), 2–24. https://doi.org/10.1111/j.1440-1738.1997.tb00038.x.

Isozaki, Y., 2019. A visage of early Paleozoic Japan: Geotectonic and paleobiogeographical significance of Greater South China. Island Arc 28 (3). https://doi.org/10.1111/iar.12296.
Isozaki, Y., Aoki, K., Nakama, T., Yanai, S., 2010. New insight into a subduction-related orogen: a reappraisal of the geotectonic framework and evolution of the Japanese Islands. Gondw. Res. 18, 82–105. https://doi.org/10.1016/j.gr.2010.02.015.
Isozaki, Y., Aoki, K., Sakata, S., Hirata, T., 2014. The eastern extension of Paleozoic South China in NE Japan evidenced by detrital zircon. GFF 136 (1), 116–119. https://doi.org/10.1080/11035897.2014.893254.
Isozaki, Y., Nakahata, H., Zakharov, Y.D., Popov, A.M., Sakata, S., Hirata, T., 2017. Greater South China extended to the Khanka block: detrital zircon geochronology of middle-upper Paleozoic sandstones in Primorye, Far East Russia. J. Asian Earth Sci. 145, 565–575. https://doi.org/10.1016/j.jseaes.2017.06.027.
Itaya, T., 2020. K–Ar phengite geochronology of HP-UHP metamorphic rocks: An in–depth review. J. Mineral. Petrol. Sci. 115 (1), 44–58. https://doi.org/10.2465/jmps.190123.
Itaya, T., Nagao, K., Inoue, K., Honjou, Y., Okada, T., Ogata, A., 1991. Argon isotope analysis by a newly developed mass spectrometric system for K–Ar dating. Mineralogical Journal 15 (5), 203–221. https://doi.org/10.2465/minerj.15.203.
Itaya, T., Tsujimori, T., 2015. White mica K–Ar geochronology of Sanbagawa eclogites from Southwest Japan: implications for deformation-controlled K–Ar closure temperature. International Geology Review 57 (5–8), 1014–1022. https://doi.org/10.1080/00206814.2014.973915.
Itaya, T., Tsujimori, T., Liou, J.G., 2011. Evolution of the Sanbagawa and Shimanto high-pressure belts in SW Japan: insights from K–Ar (Ar–Ar) geochronology. J. Asian Earth Sci. 42 (6), 1075–1090. https://doi.org/10.1016/j.jseaes.2011.06.012.
Kaneoka, I., Takaoka, N., 1980. Rare gas isotopes in Hawaiian ultramafic nodules and volcanic rocks: constraint on genetic relationships. Science 208 (4450), 1366–1368. https://doi.org/10.1126/science.208.4450.1366.
Kimura, K., Hayasaka, Y., 2019. Zircon U-Pb age and Nd isotope geochemistry of latest Neoproterozoic to early Paleozoic Oeyama ophiolite: evidence for oldest MORB-type oceanic crust in Japanese accretionary system and its tectonic implications. Lithos 342, 345–360. https://doi.org/10.1016/j.lithos.2019.06.001.
Kunugiza, K., Nakamura, E., Goto, A., Kobayashi, K., Ota, T., Miyajima, H., Yokoyama, K., 2017. In-situ U-Pb zircon age dating deciphering the formation event of the omphacite growth over relict edenitic pargasite in omphacite-bearing jadeitite of the Itoigawa-Omi area of the Hida-Gaien belt, Central Japan. J. Mineral. Petrol. Sci. 112 (5), 256–270. https://doi.org/10.2465/jmps.170402a.
Liu, Q., Yu, J.H., O'Reilly, S.Y., Zhou, M.F., Griffin, W.L., Wang, L., Cui, X., 2014. Origin and geological significance of Paleoproterozoic granites in the northeastern Cathaysia Block, South China. Precambrian Res. 248, 72–95. https://doi.org/10.1016/j.precamres.2014.04.001.
Ludwig, K.R., 2001. Squid 1.02: a User's Manual (special Publication no. 2). Berkeley Geochronology Center Publication 2, 1–19.
Maruyama, S., 1981. The Kurosegawa serpentinite melange zone and its role in the evolution of Southwest Japan. Memoir of the Geological Society of China (Taiwan) 4, 269–279.
Maruyama, S., 1997. Pacific-type orogeny revisited: Miyashiro-type orogeny proposed. Island Arc 6 (1), 91–120. https://doi.org/10.1111/j.1440-1738.1997.tb00042.x.
Maruyama, S., Banno, S., Matsuda, T., Nakajima, T., 1984. Kurosegawa zone and its bearing on the development of the Japanese Islands. Tectonophysics 110 (1–2), 47–60. https://doi.org/10.1016/0040-1951(84)90057-X.
Maruyama, S., Ueda, Y., 1975. Schist xenoliths in ultrabasic body accompanied with Kurosegawa tectonic zone in Eastern Shikoku and their K–Ar ages. The Journal of the Japanese Association of Mineralogists, Petrologists and Economic Geologists 70 (2), 47–52. https://doi.org/10.2465/ganko1941.70.47.
Miyashiro, A., 1961. Evolution of metamorphic belts. J. Petrol. 2 (3), 277–311.
Nagao, K., Nishido, H., Itaya, T., Ogata, K., 1984. An age determination by K–Ar method. Bulletin of the Hiruzen Research Institute, Okayama University of Science 9, 19–38.
Nakamizu, M., 1989. Metamorphic rocks in the Omi-Renge serpentinite mélange, Hida marginal tectonic belt, Central Japan. Memoir of the Geological Society of Japan 33, 21–35.
Nakamura, C., Enami, M., 1994. Prograde amphiboles in hematite-bearing basic and quartz schists in the Sanbagawa belt, Central Shikoku: relationship between metamorphic field gradient and P-T paths of individual rocks. J. Metam. Geol. 12 (6), 841–852. https://doi.org/10.1111/j.1525-1314.1994.tb00063.x.
Nishimura, Y., 1998. Geotectonic subdivision and areal extent of the Sangun belt, Inner Zone of Southwest Japan. J. Metam. Geol. 16 (1), 129–140. https://doi.org/10.1111/j.1525-1314.1998.00059.x.
Okamoto, A., Toriumi, M., 2005. Progress of actinolite-forming reactions in mafic schists during retrograde metamorphism: an example from the Sanbagawa metamorphic belt in Central Shikoku, Japan. J. Metam. Geol. 23 (5), 335–356. https://doi.org/10.1111/j.1525-1314.2005.00580.x.
Osanai, Y., Hamamoto, T., Kagami, H., Owada, M., Doyama, D., Ando, T., 2000. Protolith and Sm-Nd geochronology of garnet-clinopyroxene granulite and garnet amphibolite from the Kurosegawa Belt in Kyushu, Southwest Japan. Memoirs of Geological Society of Japan 56, 199–212.
Osanai, Y., Yoshimoto, A., Nakano, N., Adachi, T., Kitano, I., Yonemura, K., Sakaki, J., Tsuchiya, N., Ishizuka, H., 2014. LA-ICP-MS zircon U–Pb geochronology of Paleozoic granitic rocks and related igneous rocks from the Kurosegawa tectonic belt in Kyushu, Southwest Japan. Japanese Magazine of Mineralogical and Petrological Sciences 43 (3), 71–99. https://doi.org/10.2465/gkk.131126.
Otsuki, M., Banno, S., 1990. Prograde and retrograde metamorphism of hematitebearing basic schists in the Sanbagawa belt in Central Shikoku. J. Metam. Geol. 8 (4), 425–439. https://doi.org/10.1111/j.1525-1314.1990.tb00629.x.
Ou, Q., Lai, J.Q., Carvalho, B.B., Zi, F., Kong, H., Li, B., Jiang, Z.Q., 2019. Different response to middle-Palaeozoic magmatism during intracontinental orogenic processes: evidence from southeastern South China Block. International Geology Review 61 (12), 1504–1521. https://doi.org/10.1080/00206814.2018.1522518.
Pearce, J.A., 1982. Trace element characteristics of lavas from destructive plate boundaries. In: Thorpe, R.S. (Ed.), Orogenic Andesites. Wiley, Chichester, U.K., pp. 528–548.
Shinji, Y., Tsujimori, T., 2019. Retrograde pumpellyite in the Yunotani garnet blueschist of the Omi area, Japan: an update on the cooling path. J. Mineral. Petrol. Sci. 114 (1), 26–32. https://doi.org/10.2465/jmps.180716.
Shu, L.S., Jahn, B.M., Charvet, J., Santosh, M., Wang, B., Xu, X.S., Jiang, S.Y., 2014. Early Paleozoic depositional environment and intraplate tectono-magmatism in the Cathaysia Block (South China): evidence from stratigraphic, structural, geochemical and geochronological investigations. Am. J. Sci. 314 (1), 154–186. https://doi.org/10.2475/01.2014.05.
Sun, S.S., McDonough, W.F., 1989. Chemical and isotopic systematics of oceanic basalts: implications for mantle composition and processes. Geological Society London Special Publications 42 (1), 313–345. https://doi.org/10.1144/GSL.SP.1989.042.01.19.
Tsujimori, T., 2010. Paleozoic Subduction-related Metamorphism in Japan: New Insights and Perspectives. Journal of Geography 119 (2), 294–312. https://doi.org/10.5026/jgeography.119.294.
Tsujimori, T., 2017. Early Paleozoic jadeitites in Japan: an overview. J. Mineral. Petrol. Sci. 112, 217–226. https://doi.org/10.2465/jmps.170406a.
Tsujimori, T., Ernst, W.G., 2014. Lawsonite blueschists and lawsonite eclogites as proxies for palaeo-subduction zone processes: a review. J. Metam. Geol. 32 (5), 437–454. https://doi.org/10.1111/jmg.12057.
Tsujimori, T., Harlow, G.E., 2012. Petrogenetic relationships between jadeitite and associated high-pressure and low-temperature metamorphic rocks in worldwide jadeitite localities: A review. Eur. J. Mineral. 24 (2), 371–390. https://doi.org/10.1127/0935-1221/2012/0024-2193.
Tsujimori, T., Harlow, G.E., 2017. Jadeitite (jadeite jade) from Japan: history, characteristics, and perspectives. J. Mineral. Petrol. Sci. 112 (5), 184–196. https://doi.org/10.2465/jmps.170804.
Tsujimori, T., Ishiwatari, A., 2002. Granulite facies relics in the early Paleozoic kyanite bearing ultrabasic metacumulate in the Oeyama belt, the Inner Zone of southwestern Japan. Gondw. Res. 5 (4), 823–835. https://doi.org/10.1016/S1342-937X(05)70916-3.
Tsujimori, T., Itaya, T., 1999. Blueschist-facies metamorphism during Paleozoic orogeny in southwestern Japan: Phengite K–Ar ages of blueschist-facies tectonic blocks in a serpentinite melange beneath early Paleozoic Oeyama ophiolite. Island Arc 8 (2), 190–205. https://doi.org/10.1046/j.1440-1738.1999.00231.x.
Tsujimori, T., Liou, J.G., 2004. Metamorphic evolution of kyanite–staurolite-bearing epidote–amphibolite from the early Palaeozoic Oeyama belt, SW Japan. J. Metam. Geol. 22 (4), 301–313. https://doi.org/10.1111/j.1525-1314.2004.00515.x.
Tsujimori, T., Liou, J.G., Ernst, W.G., Itaya, T., 2006. Triassic paragonite- and garnet-bearing epidote-amphibolite from the Hida Mountains, Japan. Gondw. Res. 9 (1–2), 167–175. https://doi.org/10.1016/j.gr.2005.03.001.
Tsujimori, T., Liou, J.G., Wooden, J.L., Miyamoto, T., 2005. U-Pb dating of large zircons in low-temperature jadeitite from the Osayama serpentinite mélange, Southwest Japan: insights into the timing of serpentinization. International Geology Review 47 (10), 1048–1057. https://doi.org/10.2747/0020-6814.47.10.1048.
Tsujimori, T., Matsumoto, K., 2006. *P–T* pseudosection of a glaucophane-epidote eclogite from Omi serpentinite mélange, SW Japan: a preliminary report. The Journal of the Geological of Japan 112 (6), 402–414. https://doi.org/10.5575/geosoc.112.407.
Tsujimori, T., Nishina, K., Ishiwatari, A., Itaya, T., 2000. 403-443 Ma kyanite-bearing epidote amphibolite from the Fuko Pass metacumulate in Oeyama, the Inner Zone of southwestern Japan. J. Geol. Soc. Jpn. 106 (9), 646–649. https://doi.org/10.5575/geosoc.106.646.
Ueda, Y., Nakajima, T., Matsuoka, K., Maruyama, S., 1980. K-Ar ages of muscovite from greenstone in the Ino Formation and schists blocks associated with the Kurosegawa tectonic zone near Kochi City, Central Shikoku. The Journal of the Japanese Association of Mineralogists, Petrologists and Economic Geologists 75 (7), 230–233. https://doi.org/10.2465/ganko1941.75.230.
Uno, M., Iwamori, H., Toriumi, M., 2015. Transition from dehydration to hydration during exhumation of the Sanbagawa metamorphic belt, Japan, revealed by the continuous P–T path recorded in garnet and amphibole zoning. Contrib. Mineral. Petrol. 170, 33. https://doi.org/10.1007/s00410-015-1185-9.
Wang, Y., Zhang, A., Fan, W., Zhao, G., Zhang, G., Zhang, Y., Zhang, F., Li, S., 2011. Kwangsian crustal anatexis within the eastern South China Block: geochemical, zircon U–Pb geochronological and Hf isotopic fingerprints from the gneissoid granites of Wugong and Wuyi–Yunkai Domains. Lithos 127 (1–2), 239–260. https://doi.org/10.1016/j.lithos.2011.07.027.
Williams, I.S., 1998. U-Th-Pb Geochronology by Ion Microprobe: Reviews in Economic Geology 7, 1–35.
Yang, Q.Y., Santosh, S., Maruyama, S., Nakagawa, M., 2016. Proto-Japan and tectonic erosion: evidence from zircon geochronology of blueschist and serpentinite. Lithosphere 8 (4), 386–395. https://doi.org/10.1130/L515.1.
Yoshida, T., Taguchi, T., Ueda, H., Horie, K., Satish-Kumar, M., 2020. Early Carboniferous HP Metamorphism in the Hida Gaien Belt, Japan: Implications for the Palaeozoic tectonic history of proto-Japan. Journal of Metamorphic Geology https://doi.org/10.1111/jmg.12564.
Young, A., Flamemt, N., Maloney, K., Williams, S., Matthews, K., Zahirovic, S., Müller, R.D., 2019. Global kinematics of tectonic plates and subduction zones since the late Paleozoic Era. Geoscience Frontiers 10 (3), 989–1013. https://doi.org/10.1016/j.gsf.2018.05.011.